Indirect contributions of global fires to surface ozone through ozone-vegetation feedback

Yadong Lei[1,2], Xu Yue[3*], Hong Liao[3], Lin Zhang[4], Yang Yang[3], Hao Zhou[1,2], Chenguang Tian[1,2], Cheng Gong[2,5], Yimian Ma[1,2], Lan Gao[1,2], Yang Cao[1,2]

[1]Climate Change Research Center, Institute of Atmospheric Physics, Chinese Academy of Sciences, Beijing, 100029, China

[2]University of Chinese Academy of Sciences, Beijing, 100029, China

[3]Jiangsu Key Laboratory of Atmospheric Environment Monitoring and Pollution Control, Collaborative Innovation Center of Atmospheric Environment and Equipment Technology, School of Environmental Science and Engineering, Nanjing University of Information Science & Technology (NUIST), Nanjing, 210044, China

[4]Laboratory for Climate and Ocean–Atmosphere Studies, Department of Atmospheric and Oceanic Sciences, School of Physics, Peking University, Beijing, 100871, China

[5]State Key Laboratory of Atmospheric Boundary Layer Physics and Atmospheric Chemistry (LAPC), Institute of Atmospheric Physics, Chinese Academy of Sciences, Beijing, 100029, China

Correspondence to: Xu Yue (yuexu@nuist.edu.cn)

Abstract: Fire is an important source of ozone (O_3) precursors. The formation of surface O_3 can cause damages to vegetation and reduce stomatal conductance. Such processes can feed back to inhibit dry deposition and indirectly enhance surface O_3. Here, we apply a fully coupled chemistry-vegetation model to estimate the indirect contributions of global fires to surface O_3 through O_3-vegetation feedback during 2005-2012. Fire emissions directly increase the global annual mean O_3 by 1.2 ppbv (5.0%) with a maximum of 5.9 ppbv (24.4%) averaged over central Africa by emitting substantial number of precursors. Considering O_3-vegetation feedback, fires additionally increase surface O_3 by 0.5 ppbv averaged over the Amazon in October, 0.3 ppbv averaged over southern Asia in April, and 0.2 ppbv averaged over central Africa in April. During extreme O_3-vegetation interactions, such feedback can rise to >0.6 ppbv in these fire-prone areas. Moreover, large ratios of indirect-to-direct fire O_3 are found in eastern China (3.7%) and the eastern U.S. (2.0%), where the high ambient O_3 causes strong O_3-vegetation interactions. With likelihood of increasing fire risks in a warming climate, fires may promote surface O_3 through both direct emissions and indirect chemistry-vegetation feedbacks. Such indirect enhancement will cause additional threats to public health and ecosystem productivity.

Keywords: fires, surface ozone, dry deposition, ozone-vegetation feedback, GC-YIBs

1 Introduction

Tropospheric ozone (O_3) is a toxic air pollutant with detrimental effects on vegetation (Yue and Unger, 2014; Juráň et al., 2021). Plant stomatal uptake of O_3 decreases both chlorophyll and Rubisco contents and increases the deformity rate of chloroplasts (Booker et al., 2007; Akhtar et al., 2010; Inada et al., 2012), which further reduces the leaf area index (LAI) and gross primary productivity (GPP) of ecosystems (Karnosky et al., 2007; Ainsworth et al., 2012). Modeling studies estimated that O_3 damage reduces global GPP by 1.5%-3.6% with regional maximum reductions of 8%-20% over eastern U.S., western Europe, and eastern China (Yue and Unger, 2014; Lei et al., 2020; Zhu et al., 2021). In turn, vegetation damage also influences both the sources and sinks of O_3 through biogeochemical and biogeophysical feedbacks (Curci et al., 2009; Heald and Geddes, 2016; Fitzky et al., 2019). The damaged vegetation decreases isoprene emissions and stomatal conductance (Wittig et al., 2009; Feng et al., 2019), which influence O_3 production and dry deposition. Moreover, weakened leaf-level transpiration following O_3 damage modulates meteorological parameters, such as surface air temperature and atmospheric relative humidity, leading to substantial biogeophysical feedbacks on surface O_3 (Lombardozzi et al., 2012; Sadiq et al., 2017).

Interactions between air pollution and terrestrial ecosystems remain challenging due to limited process-based knowledge and the separate development of chemistry and vegetation models (He et al., 2020). At present, the feedbacks from O_3-damaging vegetation on O_3 have only been examined by four papers (Sadiq et al., 2017; Zhou et al., 2018; Gong et al., 2020; Zhu et al., 2021). Sadiq et al. (2017) implemented a parameterization of O_3 vegetation damage into a climate model and quantified online O_3-vegetation coupling. Simulations showed that surface O_3 could be enhanced by up to 4-6 ppbv over Europe, North America, and China through comparable effects from biogeochemical (decreased dry deposition and increased isoprene emissions) and biogeophysical (changes in meteorological variables following reduced transpiration rate) feedbacks from O_3-vegetation interactions. Similar conclusions were achieved by Zhu et al. (2021), who investigated the effects of O_3-vegetation interaction in China using a two-way coupled land-atmosphere model. By including O_3 damage to isoprene emissions in a fully coupled global chemistry–carbon–climate model, Gong et al. (2020) highlighted that such O_3-vegetation positive feedbacks were mainly driven by reduced dry deposition following O_3 damage to photosynthesis. Different from above three studies, Zhou et al. (2018) implemented steady-state O_3-induced LAI changes into GEOS-Chem and quantified only the influences of O_3-vegetation biogeochemical feedbacks because the model is driven with prescribed meteorological fields. Results showed that O_3-induced damage to LAI can enhance O_3 by up to 3 ppbv in the tropics, eastern North America, and southern China through changes in dry deposition and isoprene emissions. All studies revealed strong positive O_3-vegetation feedback to surface O_3, though the magnitudes are different due to discrepancies in O_3 damaging schemes, as well as differences in the models.

Fire plays an important role in disturbing the terrestrial carbon budget (Bond-Lamberty et al., 2007; Amiro et al., 2009; Turetsky et al., 2011; Yue and Unger, 2018). Global fires directly emit 2-3 Pg (1 Pg = 10^{15} g) carbon into the atmosphere every year (van der Werf et al., 2010). Moreover, fires contribute to the production of tropospheric O_3 by emitting substantial number of precursors (Cheng et al., 1998; Kita et al., 2000; Oltmans et al., 2010; Jaffe et al., 2013; Lu et al., 2016). Globally, fires account for 3-5% of the total tropospheric O_3 (Bey et al., 2001; Ziemke et al., 2009; Jaffe and Wigder, 2012). Regionally, especially in Amazon and central Africa, fires can enhance surface O_3 by 10-30 ppbv through emissions of NO_x and VOCs during fire seasons (Yue and Unger, 2018; Pope et al., 2020). Over these regions, strong O_3-vegetation interactions are expected because of high fire O_3 concentrations and dense vegetation cover. Previous studies showed that fire O_3 causes large GPP reduction of 200-400 Tg C yr^{-1} over Amazon and central Africa (Pacifico et al., 2015; Yue and Unger, 2018). With likely increased wildfire activity due to global warming, surface O_3 will be further enhanced by wildfires (Amiro et al., 2009; Balshi et al., 2009; Wang et al., 2016; Yue et al., 2017), leading to more severe O_3 damage on vegetation. Although the feedback of vegetation damage on surface O_3 have been well explored on global (Sadiq et al., 2017; Zhou et al., 2018; Gong et al., 2020) or regional (Zhu et al., 2021) scales, these studies all focused on O_3-vegetation from combined anthropogenic and natural sources. Therefore, quantification of the O_3-vegetation interactions associated with fire emissions is very important for a comprehensive understanding of the effects of fires on surface O_3.

Here, we apply a fully coupled chemistry-vegetation model (GEOS-Chem-YIBs, hereafter referred to as GC-YIBs) to examine the indirect contributions of fires to surface O_3. Fire-induced O_3 affects plant photosynthesis and stomatal conductance. In turn, predicted changes in LAI and canopy stomatal conductance influence both the sources and sinks of tropospheric O_3. Such O_3-vegetation interactions result in additional enhancement in surface O_3 caused by fire emissions (Fig. 1). Section 2 describes the GC-YIBs model and sensitivity experiments conducted in this study. Section 3 quantifies the feedbacks of fire-induced O_3 vegetation damage on surface O_3 concentrations. The last section summarizes the findings and discusses the uncertainties.

2 Materials and Methods

2.1 The GC-YIBs model

GC-YIBs is a coupled chemistry-vegetation model developed by implementing the Yale Interactive terrestrial Biosphere (YIBs) model into GEOS-Chem version 12.0.0 (Lei et al., 2020). GEOS-Chem is a widely used global 3-D chemical transport model (CTM) for simulating atmospheric composition and air quality (Yue et al., 2015; Yan et al., 2018; David et al., 2019; Lu et al., 2019). This model uses a detailed HO_x-NO_x-VOC-O_3-halogen-aerosol tropospheric chemistry to simulate tropospheric O_3 fluxes (Barret et al., 2016; Gong and Liao, 2019), while a simplified linearized Linoz chemistry mechanism is applied to simulate stratospheric O_3 (McLinden et al., 2000). Aerosols simulated in GEOS-Chem include secondary inorganic aerosols, secondary organic aerosols, primary organic aerosols, black carbon, dust, and sea salt (Dang and Liao, 2019; Li et al., 2019). The gas-aerosol partitioning of the sulfate–nitrate–ammonium system is computed by the ISORROPIA v2.0 thermodynamic equilibrium model (Fountoukis and Nenes, 2007). The atmospheric emissions from different sources, regions, and species on a user-defined grid are calculated through the online Harvard NASA Emissions Component (HEMCO) module (Keller et al., 2014). HEMCO is highly customizable in that it can automatically combinate, overlay, and update emission inventories and scale factors specified by the users. In general, the GEOS-Chem model overestimates summer surface O_3 concentrations in the eastern U.S. and China (Zhang et al., 2011; Travis et al., 2016; Schiferl and Heald, 2018).

YIBs is a vegetation model designed to dynamically simulate the changes in LAI and tree height based on carbon assimilation, respiration, and allocation processes (Yue and Unger, 2015). The model computes carbon uptake for 9 vegetation types, including evergreen needleleaf forest, deciduous broadleaf forest, evergreen broadleaf forest, shrubland, tundra, C_3/C_4 grasses, and C_3/C_4 crops. The canopy is divided into an adaptive number of layers (typically 2-16) for light stratification. The YIBs model applies a well-established Michaelis–Menten enzyme kinetics scheme to compute the leaf photosynthesis (Farquhar et al., 1980; Von Caemmerer and Farquhar, 1981), which is further upscaled to the canopy level by the separation of sunlit and shaded leaves (Spitters, 1986). The LAI and carbon allocation schemes are from the TRIFFID model (Clark et al., 2011). Previous studies have shown that the YIBs model has good performance in simulating the spatial pattern and temporal variability of GPP and LAI based on site observations and satellite products (Yue and Unger, 2015, 2018).

The GC-YIBs model links atmospheric chemistry and vegetation in a two-way coupling. As a result, changes in chemical components or vegetation will simultaneously feed back to influence the other systems. In this study, the GC-YIBs model is driven with the meteorological fields from the Modern-Era Retrospective analysis for Research and Applications, version 2 (MERRA2) with a horizontal resolution of 4° latitude by 5° longitude, as well as 47 vertical layers from the surface to 0.01 hPa. Within GC-YIBs, the online-simulated surface O_3 in GEOS-Chem affects photosynthesis and canopy stomatal conductance; in turn, the online-simulated vegetation parameters, such as LAI and stomatal conductance, in YIBs, affect both the sources and sinks of O_3 by altering precursor emissions and dry deposition at the 1-hour integration time step. An earlier study evaluated the GC-YIBs model and showed good performance in simulating surface O_3, GPP, LAI, and O_3 dry deposition (Lei et al., 2020).

2.2 Scheme of O_3 vegetation damage

The GC-YIBs model calculates the impacts of O_3 exposure on photosynthesis based on a semi-mechanistic scheme (Sitch et al., 2007):

$$A' = \alpha \cdot A \quad (1)$$

where A' and A represent the O_3-damaging and original leaf photosynthesis, respectively. The O_3 damage factor is represented by α; O_3 can cause damage to photosynthesis only if $\alpha < 1$. The factor α is calculated as a function of excessive O_3 flux and damaging sensitivity coefficient (β):

$$\alpha = -\beta \cdot max\left(F_{O_3} - T_{O_3}, 0\right) \quad (2)$$

The coefficient β can have two values for each vegetation type (Table S1), indicating low to high O_3 damaging sensitivities (Sitch et al., 2007). T_{O_3} represents the O_3 flux threshold, reflecting the O_3 tolerance of different vegetation types. F_{O_3} represents the stomatal O_3 flux and is calculated based on ambient $[O_3]$, aerodynamic resistance (r_a), boundary layer resistance (r_b) and stomatal resistance (r_s):

$$F_{O_3} = \frac{[O_3]}{r_a + r_b + k \cdot r_s'} \quad (3)$$

Here k represents the ratio of leaf resistance for O_3 to leaf resistance for water vapor. Parameters r_a and r_b are calculated by the GEOS-Chem model. O_3-damaging leaf photosynthesis (A') is then integrated over all canopy layers to generate O_3-damaging GPP:

$$GPP' = \int_0^{LAI} A' \, dL \quad (4)$$

The O_3-damaging stomatal resistance (r_s') is calculated based on the model of Ball and Berry (Baldocchi et al., 1987):

$$\frac{1}{r_s'} = g_s' = m\frac{A_{net}' \cdot RH}{c_s} + b \quad (5)$$

where m and b represent the slope and intercept of empirical fitting to the Ball-Berry stomatal conductance equation, respectively. A_{net}' represents

O_3-damaging net leaf photosynthesis, RH represents the relative humidity and c_s is the ambient CO_2 concentration. Previous studies have shown that this scheme within the framework of YIBs can reasonably capture the response of GPP and stomatal conductance to surface [O_3] based on hundreds of global observations (Yue et al., 2016; Yue and Unger, 2018).

2.3 Fire emissions

Fire Inventory from NCAR (FINN) version 1.5 is used by GC-YIBs to simulate fire-induced perturbations in O_3. FINN provides daily global emissions of many chemical species from open biomass burning at a resolution of 1 km^2 (Wiedinmyer et al., 2011). The inventory estimates fire locations and biomass burned using satellite observations of active fires and land cover, together with emission factors and fuel loadings. For each land type, emission factors for different gaseous and particulate species are taken from measurements (Andreae and Merlet, 2001; Andreae and Rosenfeld, 2008; Akagi et al., 2011). Daily fire emissions for 2002-2012 are available at http://bai.acom.ucar.edu/Data/fire/. In GC-YIBs, all biomass burning emissions occur in the atmospheric boundary layer. Such configuration might slightly overestimate regional O_3 formation as observations suggested ~20% of fire plumes reached the height above the boundary layer (Val Martin et al., 2010) and consequently enhanced surface O_3 level at the downwind regions (Jaffe and Wigder, 2012). The FINN inventory has been widely used in regional and global chemical transport models (e.g., WRF-Chem and GEOS-Chem) to quantify the impacts of fires on air quality and weather (Jiang et al., 2012; Nuryanto, 2015; Vongruang et al., 2017; Brey et al., 2018; Watson et al., 2019).

2.4 Site-level measurements

Measurements of surface [O_3] in the U.S. are provided by Air Quality System (AQS, https://www.epa.gov/aqs), those over Europe are provided by European Monitoring and Evaluation Programme (EMEP, https://emep.int). The observed [O_3] at Manaus, Tg Malim, and Welgegund sites are from earlier studies (Ahamad et al., 2014; Laban et al., 2018; Pope et al., 2020).

2.5 Model simulations

In this study, eight simulations (Table 1) are performed to examine both the direct and indirect contributions of fires to surface O_3. These simulations can be divided into two main groups:

1. CTRL_FIRE and CTRL_NOFIRE are the control runs using the same emissions except that the latter omits fire emissions. These runs calculate and output offline O_3 damage, which decreases instantaneous leaf photosynthesis but does not feed back to affect plant growth and O_3 dry deposition.
2. O3CPL_FIRE and O3CPL_NOFIRE are the sensitive experiments that consider online coupling between O_3 and vegetation. These runs include online O_3 damage to plant photosynthesis, which feeds back to affect both vegetation and air pollution. The two simulations apply the same emissions, except that the latter

omits fire emissions.

For each of these four configurations, two runs are conducted with either high (HS) or low (LS) O_3 damaging sensitivities. All simulations are performed from 2002-2012 using the GC-YIBs model driven by MERRA2 meteorological fields. The first 3 years are used as spin up, and the results of the last 8 years are analyzed. For the same configurations, the results from low and high O_3 damaging sensitivities are averaged. The differences between CTRL_NOFIRE and O3CPL_NOFIRE represent the surface O_3 enhancements through O_3-vegetation feedback without fire emissions. The differences between CTRL_FIRE and CTRL_NOFIRE, named O3OFF, represent the direct contributions of fires to surface O_3. The differences between O3CPL_FIRE and O3CPL_NOFIRE, named O3CPL, represent both direct and indirect contributions of fires to surface O_3. The differences between O3CPL and O3OFF represent the indirect contributions of fires to surface O_3 through O_3-vegetation interactions. It should be noted that only biogeochemical feedbacks from O_3 vegetation damage on surface O_3 are considered in this study because GC-YIBs uses prescribed meteorology (MERRA2).

3 Results

3.1 Model validation

Simulated surface daily maximum 8-hour average O_3 concentrations (MDA8 [O_3], short for [O_3] hereafter) are evaluated using measurements from the AQS and EMEP datasets over the period of 2005-2012 (Fig 2). The model well captures the observed spatial distribution of annual [O_3] in the U.S. and Europe, with a high correlation coefficient of 0.51 ($p<0.01$). Although GC-YIBs overestimates the [O_3] in the eastern U.S. while underestimating it in western Europe, the normalized mean bias (NMB) is only 4.0%, with a root mean square error (RMSE) of 5.4 ppbv. Therefore, the simulated O_3 vegetation damage in our study is slightly overestimated in the eastern U.S. but underestimated in western Europe.

3.2 Direct contributions of fires to O_3

Without fire emissions, the simulated global mean [O_3] is 23.9 ppbv, with a grid maximum of 63.7 ppbv over the Beijing–Tianjin–Hebei region averaged for 2005-2012 (Fig. 3a). Most high [O_3] is distributed in the Northern Hemisphere, where anthropogenic emissions make the dominant contributions. The inclusion of fire emissions increases global annual [O_3] by an average of 1.2 ppbv (5.0%). Regionally, the largest enhancement of [O_3] by 5.9 ppbv (24.4%) is averaged over central Africa, with smaller enhancements of 5.7 ppbv (38.2%) averaged over the Amazon, and 3.8 ppbv (10.2%) averaged over southern Asia. Smaller enhancements of 1.1 ppbv (2.2%), 0.9 ppbv (2.1%), and 0.8 ppbv (2.2%) are averaged respectively over eastern China, western Europe, and the eastern U.S. (Fig. 3b). The predicted fire-induced enhancements in [O_3] agree well with the simulations using the same model but with fire emissions from the Global Fire Emission Database (GFED) version 3 (Yue and Unger, 2018).

We further evaluated the model performance in simulating fire-induced $\Delta[O_3]$ at three sites across biomass burning regions (Fig. S1). Without fire emissions, the $[O_3]$ is obviously underestimated, with NMBs of -25.5% at Tg Malim, -53.6% at Manaus, and -21.3% at Welgegund. As a comparison, simulations with fire emissions show NMBs in fire seasons of -8.7% at Tg Malim, -1.4% at Manaus, and -15.1% at Welgegund, suggesting improved O_3 simulations by including fire emissions.

3.3 Fire-induced O_3 damages to GPP

Surface O_3 causes strong damage to ecosystem productivity (Fig. 4). Without fire emissions, surface O_3 reduces global annual GPP by 1.7% (3899.8 Tg C yr^{-1}, Figs. 4a and 4c). Regional maximum reductions of 10.9% (372.0 Tg C yr^{-1}), 6.1% (366.1 Tg C yr^{-1}), and 4.9% (323.8 Tg C yr^{-1}) are averaged respectively over eastern China, the eastern U.S., and western Europe; these reductions are attributed to the high ambient $[O_3]$ level and the large stomatal conductance over these regions. The patterns of O_3-induced GPP reductions agree with previous estimates using the same O_3 damage schemes (Sitch et al., 2007; Yue and Unger, 2015). However, compared to simulations using another scheme (Lombardozzi et al., 2012; Zhou et al., 2018; Zhu et al., 2021), this study estimates smaller GPP reductions. Such discrepancy indicates there are large uncertainties in O_3 vegetation damage schemes, and more observations should be developed to evaluate different schemes in future studies.

The inclusion of fire emissions causes additional GPP reductions. Globally, fire-induced ΔO_3 decreases annual GPP by 0.4% (1312.0 Tg C yr^{-1}, Figs. 4b and 4d). Regionally, the largest GPP reduction of 1.4% (370.3 Tg C yr^{-1}) is averaged over the Amazon due to the largest enhancement of [O_3] caused by fires. Furthermore, fire Δ[O_3] causes additional annual GPP reductions of 1.3% (358.0 Tg C yr^{-1}), averaged over central Africa, and 1.0% (77.1 Tg C yr^{-1}), averaged over southern Asia. In contrast, limited damage is found in eastern China, western Europe, and the eastern U.S. due to low fire Δ[O_3]. Following the changes in GPP, fire-induced O_3 damage to LAI shows a regional maximum of 0.3-0.7% in central Africa and a global reduction of 0.02-0.5% (Fig. S2).

3.4 Indirect contributions of fires to O_3

Vegetation parameters such as LAI and stomatal conductance play important roles in modulating surface [O_3]. The O_3-induced changes in these variables interactively feed back to alter local [O_3] (Fig. 5). Without fire emissions, the annual Δ[O_3] from O_3-vegetation interactions is limited to eastern China by 0.5 ppbv, the eastern U.S. by 0.3 ppbv, and western Europe by 0.2 ppbv. The largest grid positive feedback of up to 0.8 ppbv is found in the eastern U.S. (Figs. 5a and 5c). Sensitivity experiments further show that such enhancement of surface [O_3] mainly results from the inhibition of stomatal conductance following reduced photosynthesis by O_3 damage (Fig. S3a). Consequently, large Δ[O_3] (Figs. 5a and 5c) are collocated with areas enduring high levels of O_3 vegetation damage (Figs. 4a and 4c). As a comparison, the feedback of

LAI changes is generally small (Fig. S3b), which is mainly attributed to limited O_3 damage on LAI (Fig. S2). The enhancement of [O_3] from fires causes additional feedback to the surface [O_3]. The largest annual Δ[O_3] of 0.13 ppbv due to O_3-vegetation feedback is averaged on over the Amazon (Figs. 5b and 5d), where the highest GPP reductions by fire-induced O_3 are predicted (Figs. 4b and 4d). Such feedback additionally enhances local [O_3] by 0.12 ppbv, averaged over central Africa, and 0.09 ppbv, averaged over southern Asia. However, limited O_3-vegetation feedback is found in the eastern U.S., eastern China, and western Europe, either because of low fire-induced Δ[O_3] (Fig. 3b) or low ΔGPP (Figs. 4b and 4d). The changes in O_3 dry deposition velocity broadly match the pattern of O_3-vegetation feedback (Fig. S4), suggesting that reduced dry deposition velocity due to O_3-induced inhibition of stomatal conductance is the dominant driver for the enhanced surface [O_3].

Fig. 6 shows seasonal variations in O_3-vegetation feedback. Without fire emissions, O_3-vegetation feedback in eastern China, the eastern U.S., and western Europe shows similar seasonal variations, increasing from January to July and then decreasing (Fig. 6a). For these regions, surface [O_3] and stomatal conductance reach maximums during the growth season (May-October), resulting in instantaneous O_3 uptake. Therefore, O_3-vegetation interactions are expected to be stronger during the growth season in the Northern Hemisphere. However, O_3-vegetation feedback driven by fires in the Amazon and Southern Asia reaches a maximum during August-December and February-June, respectively. Moreover, double peaks are shown in central Africa, with maximums during February-April and July-September (Fig. 6b). The distinct seasonal variations in biomass burning regions are attributed to fire emissions. At low latitudes, stomatal conductance shows limited seasonal variations. Therefore, O_3-vegetation feedback driven by fires is mainly dependent on fire-induced $\Delta[O_3]$.

Fire-induced O_3 shows stronger interactions with vegetation under favorable meteorological conditions. We sort daily $\Delta[O_3]$ from O_3-vegetation feedback and calculate the average of $\Delta[O_3]$ above the 95^{th} percentile (Fig. S5). The spatial pattern of $\Delta[O_3]$ during extreme O_3-vegetation feedback is broadly consistent with that of the annual average, albeit with much stronger O_3-vegetation feedback. Without fire emissions, O_3-vegetation feedback enhances $[O_3]$ by 2.0 ppbv averaged over eastern China, 1.8 ppbv averaged over the eastern U.S., and 1.1 ppbv averaged over western Europe (Figs. S5a and S5c). Fire emissions alone enhance $[O_3]$ through O_3-vegetation interactions by 1.1 ppbv averaged over the Amazon, 0.8 ppbv averaged over southern Asia, and 0.6 ppbv averaged over central Africa during extreme O_3-vegetation feedback (Figs. S5b and S5d).

3.5 Indirect vs. direct contributions of fires to O_3

We further compare the indirect and direct contributions of fire emissions to surface $[O_3]$. Here, the direct contributions indicate $\Delta[O_3]$ caused by fire emissions of chemical precursors, while the indirect contributions represent additional $\Delta[O_3]$ from O_3-vegetation interactions caused by fire-induced O_3. Without fire emissions,

O_3-vegetation interactions cause enhancement of [O_3] by 1.0% averaged over eastern China, 0.8% averaged over the eastern U.S., and 0.5% averaged over western Europe (Figs. 7a and 7c). Compared to nonfire sources, fire emissions cause larger relative perturbations in surface [O_3] through O_3-vegetation interactions (Figs. 7b and 7d). The ratios of indirect to direct annual Δ[O_3] are 3.7% averaged over eastern China, 2.0% averaged over the eastern U.S., and 1.6% averaged over western Europe. For these regions, the absolute Δ[O_3] from direct fire emissions is usually lower than 1 ppbv (Fig. 3b). However, the high level of background [O_3] (all sources except fire emissions, Fig. 3a) provides such a sensitive environment that the moderate increases of [O_3] from fires can cause large feedback to regional surface [O_3] through vegetation damage. For fire-prone regions, the ratios of indirect to direct annual Δ[O_3] are 2.6% averaged over southern Asia, 1.9% averaged over the eastern U.S., and 1.4% averaged over central Africa.

3.6 Aggravated O_3 damage to GPP through O_3-vegetation feedback

The additional O_3 enhancement can exacerbate the damaging effects on vegetation. Without fire emissions, online O_3 causes a global annual GPP reduction of 0.2% (299.6 Tg C yr^{-1}, Figs. S6a and S6c) from the offline O_3. Regionally, additional reductions are mainly found in eastern China, the eastern U.S., and western Europe, where GPP is further decreased by 27.1 Tg C yr^{-1}, 40.8 Tg C yr^{-1} and 28.4 Tg C yr^{-1}, respectively. For fire emissions, the online fire-induced ΔO_3 results in a higher GPP reduction by 25.0 Tg C yr^{-1} averaged over the Amazon, and 24.3 Tg C yr^{-1} averaged over central Africa, and 7.1 Tg C yr^{-1} averaged over southern Asia compared to the offline fire-induced ΔO_3 (Figs. S6b and S6d). Such spatial patterns are broadly consistent with $\Delta[O_3]$ induced by O_3-vegetation feedback (Fig. 5).

4 Conclusions and discussion

Many studies have explored the direct contributions to surface O_3 by fire emissions. However, the feedback of fire-induced O_3 vegetation damage to surface $[O_3]$ remains unquantified. In this study, we find that fire-induced O_3 causes a positive feedback to surface $[O_3]$ mainly because of the inhibition effects on stomatal conductance. Regionally, O_3-vegetation feedback driven by fires enhances surface annual $[O_3]$ by 0.13 ppbv averaged over the Amazon, 0.12 ppbv averaged over central Africa, and 0.09 ppbv averaged over southern Asia. Such feedback exhibit large seasonal variations, with the maximums of 0.5 ppbv averaged over the Amazon in October, 0.3 ppbv averaged over southern Asia in April, and 0.2 ppbv averaged over central Africa in April. During extreme O_3-vegetation interactions, the feedback can rise to >0.6 ppbv in these fire-prone areas. Although direct formations of O_3 from fires are limited in eastern China and the eastern U.S., the feedback of O_3-vegetation coupling results in additional enhancement of surface $[O_3]$ by 3.7% and 2.0% upon the fire-induced $\Delta[O_3]$. Such large ratios in these regions are attributed to the high level of ambient $[O_3]$ that provides a sensitive environment in which moderate increases in $[O_3]$ from fires can cause large indirect contributions to regional $[O_3]$ through vegetation damage.

Some uncertainties may affect the conclusions of this study. (i) The GC-YIBs simulations do not consider the direct fire damages to vegetation and the consequent long-term recovery of forests. In our study, we focus only on the feedbacks of fire-induced O_3-vegetation interactions to surface O_3. (ii) Fires can decrease VOC emissions from biogenic sources by damaging vegetation directly. However, compared to the VOCs emitted by fires, the VOC loss from burned vegetation is generally smaller (Fig. S7). Therefore, the influence of reduced VOCs from vegetation loss on surface [O_3] can be ignored. (iii) There is evidence that O_3 exposure may cause "sluggishness" that delays the stomatal responses to O_3 damage (Huntingford et al., 2018). However, we do not include "sluggishness" in our scheme because its net impacts on stomatal conductance remain uncertain. For example, observations found that the increased short-term water loss (delayed stomatal responses) may be offset by the decreased long-term water loss (lower steady-state stomatal conductance) with the stomatal "sluggishness" (Paoletti et al., 2019). (iv) We employed a model resolution of 4°×5° due to the limitations in computational resources. We performed a one-year sensitivity simulation at a 2°×2.5° resolution. The comparisons show that fire-induced direct O_3 enhancement is very similar between the simulations with low and high resolutions, although the former runs predict slightly higher changes in [O_3] than the latter (Fig. S8). (v) different biomass burning datasets may affect the estimated O_3-vegetation feedback in our study. At present, the FINNv1.5 and GFEDv4.1 inventories are available in the public-release of GEOS-Chem v12.0.0. Compared with the FINNv1.5 inventory, simulations using the GFEDv4.1 inventory predict a lower O_3-vegetation feedback in the Amazon (Fig. S9a) and southern Asia (Fig. S9c) but a higher O_3-vegetation feedback in central Africa (Fig. S9b).

Despite these uncertainties, we present the first estimate of O_3 enhancement by fire emissions through O_3-vegetation interactions. Such enhancement is not limited to fire-prone regions, but is also significant over downwind areas with high ambient [O_3] levels. Although the absolute perturbations may be moderate for the whole fire season, O_3-vegetation interactions can largely increase surface O_3 during extreme O_3-vegetation interactions, leading to additional threats to public health and ecosystem productivity.

Data availability

The site-level [O_3] in the U.S. can be download from AQS (https://www.epa.gov/aqs). The site-level [O_3] in the Europe can be download from EMEP (https://emep.int). The observed [O_3] at Manaus, Tg Malim, and Welgegund sites are from earlier studies (Ahamad et al., 2014; Laban et al., 2018; Pope et al., 2020). The GC-YIBs simulation results are available from the corresponding authors on request.

Competing interests. The authors declare no competing financial interests.

Author Contributions. XY conceived the study. YL conducted the model simulations. YL and XY were responsible for results analysis. HL, LZ, and YY revised and improved the manuscript. HZ, CT, and CG helped prepare model input. YM, LG, and YC helped prepare observation dataset.

Acknowledgements. This work was jointly supported by Jiangsu Science Fund for Distinguished Young Scholars (grant no. BK20200040) and the National Natural Science Foundation of China (grant no. 41975155).

References

Ahamad, F., Latif, M. T., Tang, R., et al. Variation of surface ozone exceedance around Klang Valley, Malaysia. Atmospheric research[J]: 2014, 139: 116-127.

Ainsworth, E. A., Yendrek, C. R., Sitch, S., et al. The Effects of Tropospheric Ozone on Net Primary Productivity and Implications for Climate Change. Annual Review of Plant Biology, Vol 63[J]: 2012, 63: 637-661.

Akagi, S., Yokelson, R. J., Wiedinmyer, C., et al. Emission factors for open and domestic biomass burning for use in atmospheric models. Atmospheric Chemistry and Physics[J]: 2011, 11: 4039-4072.

Akhtar, N., Yamaguchi, M., Inada, H., et al. Effects of ozone on growth, yield and leaf gas exchange rates of two Bangladeshi cultivars of wheat (Triticum aestivum L.). Environmental Pollution[J]: 2010, 158: 1763-1767.

Amiro, B. D., Cantin, A., Flannigan, M. D., et al. Future emissions from Canadian boreal forest fires. Canadian Journal of Forest Research[J]: 2009, 39: 383-395.

Andreae, M. and Rosenfeld, D. Aerosol–cloud–precipitation interactions. Part 1. The nature and sources of cloud-active aerosols. Earth-Science Reviews[J]: 2008, 89: 13-41.

Andreae, M. O. and Merlet, P. Emission of trace gases and aerosols from biomass burning. Global biogeochemical cycles[J]: 2001, 15: 955-966.

Baldocchi, D. D.,Hicks, B. B. and Camara, P. A Canopy Stomatal-Resistance Model for Gaseous Deposition to Vegetated Surfaces. Atmospheric Environment[J]: 1987, 21: 91-101.

Barret, B., Sauvage, B., Bennouna, Y., et al. Upper-tropospheric CO and O_3 budget during the Asian summer monsoon. Atmos. Chem. Phys[J]: 2016, 16: 9129-9147.

Bey, I., Jacob, D. J., Logan, J. A., et al. Asian chemical outflow to the Pacific in spring: Origins,

pathways, and budgets. Journal of Geophysical Research-Atmospheres[J]: 2001, 106: 23097-23113.
Bond-Lamberty, B., Peckham, S. D., Ahl, D. E., et al. Fire as the dominant driver of central Canadian boreal forest carbon balance. Nature[J]: 2007, 450: 89-92.
Booker, F. L., Burkey, K. O., Pursley, W. A., et al. Elevated carbon dioxide and ozone effects on peanut: I. Gas-exchange, biomass, and leaf chemistry. Crop Science[J]: 2007, 47: 1475-1487.
Brey, S. J., Barnes, E. A., Pierce, J. R., et al. Environmental Conditions, Ignition Type, and Air Quality Impacts of Wildfires in the Southeastern and Western United States. Earth's Future[J]: 2018, 6: 1442-1456.
Cheng, L., McDonald, K. M., Angle, R. P., et al. Forest fire enhanced photochemical air pollution. A case study. Atmospheric Environment[J]: 1998, 32: 673-681.
Clark, D., Mercado, L., Sitch, S., et al. The Joint UK Land Environment Simulator (JULES), model description—Part 2: carbon fluxes and vegetation dynamics. Geoscientific Model Development[J]: 2011, 4: 701-722.
Curci, G., Beekmann, M., Vautard, R., et al. Modelling study of the impact of isoprene and terpene biogenic emissions on European ozone levels. Atmospheric Environment[J]: 2009, 43: 1444-1455.
Dang, R. and Liao, H. Severe winter haze days in the Beijing–Tianjin–Hebei region from 1985 to 2017 and the roles of anthropogenic emissions and meteorology. Atmospheric Chemistry and Physics[J]: 2019, 19: 10801-10816.
David, L. M., Ravishankara, A., Brewer, J. F., et al. Tropospheric ozone over the Indian subcontinent from 2000 to 2015: Data set and simulation using GEOS-Chem chemical transport model. Atmospheric Environment[J]: 2019, 219: 117039.
Farquhar, G. D.,von Caemmerer, S. v. and Berry, J. A. A biochemical model of photosynthetic CO_2 assimilation in leaves of C_3 species. Planta[J]: 1980, 149: 78-90.
Feng, Z. Z., Yuan, X. Y., Fares, S., et al. Isoprene is more affected by climate drivers than monoterpenes: A meta-analytic review on plant isoprenoid emissions. Plant Cell and Environment[J]: 2019, 42: 1939-1949.
Fitzky, A. C., Sandén, H., Karl, T., et al. The interplay between ozone and urban vegetation–BVOC emissions, ozone deposition and tree ecophysiology. Frontiers in Forests and Global Change[J]: 2019, 2: 50.
Fountoukis, C. and Nenes, A. ISORROPIA II: a computationally efficient thermodynamic equilibrium model for K^+- Ca^{2+}-Mg^{2+}-NH_4^+-Na^+-SO_4^{2-} NO_3^--Cl^--H_2O aerosols. Atmospheric Chemistry and Physics[J]: 2007, 7: 4639-4659.
Gong, C., Lei, Y., Ma, Y., et al. Ozone-vegetation feedback through dry deposition and isoprene emissions in a global chemistry-carbon-climate model. Atmospheric Chemistry and Physics[J]: 2020, 20: 3841-3857.
Gong, C. and Liao, H. A typical weather pattern for ozone pollution events in North China. Atmospheric Chemistry and Physics[J]: 2019, 19: 13725-13740.
He, C.,Clifton, O. and Coauthors. Interactions between Air Pollution and Terrestrial Ecosystems: Perspectives on Challenges and Future Directions. Bulletin of the American Meteorological Society[J]: 2020, doi: doi: https://doi.org/10.1175/BAMS-D-20-0066.1., 2020.
Heald, C. L. and Geddes, J. A. The impact of historical land use change from 1850 to 2000 on secondary particulate matter and ozone. Atmospheric Chemistry and Physics[J]: 2016, 16:

14997-15010.

Huntingford, C., Oliver, R. J., Mercado, L. M., et al. Technical note: A simple theoretical model framework to describe plant stomatal “sluggishness” in response to elevated ozone concentrations. Biogeosciences[J]: 2018, 15: 5415-5422.

Inada, H., Kondo, T., Akhtar, N., et al. Relationship between cultivar difference in the sensitivity of net photosynthesis to ozone and reactive oxygen species scavenging system in Japanese winter wheat (Triticum aestivum). Physiologia Plantarum[J]: 2012, 146: 217-227.

Jaffe, D. A., Wigder, N., Downey, N., et al. Impact of wildfires on ozone exceptional events in the Western US. Environ Sci Technol[J]: 2013, 47: 11065-11072.

Jaffe, D. A. and Wigder, N. L. Ozone production from wildfires: A critical review. Atmospheric Environment[J]: 2012, 51: 1-10.

Jiang, X. Y.,Wiedinmyer, C. and Carlton, A. G. Aerosols from Fires: An Examination of the Effects on Ozone Photochemistry in the Western United States. Environmental Science & Technology[J]: 2012, 46: 11878-11886.

Juráň, S.,Grace, J. and Urban, O. Temporal Changes in Ozone Concentrations and Their Impact on Vegetation. Atmosphere[J]: 2021, 12: 82.

Karnosky, D. F., Skelly, J. M., Percy, K. E., et al. Perspectives regarding 50 years of research on effects of tropospheric ozone air pollution on US forests. Environmental Pollution[J]: 2007, 147: 489-506.

Keller, C. A., Long, M. S., Yantosca, R. M., et al. HEMCO v1. 0: a versatile, ESMF-compliant component for calculating emissions in atmospheric models. Geosci. Model Dev.[J]: 2014, 7: 1409-1417.

Kita, K.,Fujiwara, M. and Kawakami, S. Total ozone increase associated with forest fires over the Indonesian region and its relation to the El Nino-Southern oscillation. Atmospheric Environment[J]: 2000, 34: 2681-2690.

Laban, T. L., Van Zyl, P. G., Beukes, J. P., et al. Seasonal influences on surface ozone variability in continental South Africa and implications for air quality. Atmospheric Chemistry and Physics[J]: 2018, 18: 15491-15514.

Lei, Y., Yue, X., Liao, H., et al. Implementation of Yale Interactive terrestrial Biosphere model v1.0 into GEOS-Chem v12.0.0: a tool for biosphere-chemistry interactions. Geoscientific Model Development[J]: 2020, 13: 1137-1153.

Li, S., Chen, L., Huang, G., et al. Retrieval of surface $PM_{2.5}$ mass concentrations over North China using visibility measurements and GEOS-Chem simulations. Atmospheric Environment[J]: 2019, 2019. 117121.

Lombardozzi, D., Levis, S., Bonan, G., et al. Predicting photosynthesis and transpiration responses to ozone: decoupling modeled photosynthesis and stomatal conductance. Biogeosciences[J]: 2012, 9: 3113-3130.

Lu, X., Zhang, L., Chen, Y., et al. Exploring 2016-2017 surface ozone pollution over China: source contributions and meteorological influences. Atmospheric Chemistry and Physics[J]: 2019, 19: 8339-8361.

Lu, X., Zhang, L., Yue, X., et al. Wildfire influences on the variability and trend of summer surface ozone in the mountainous western United States. Atmospheric Chemistry and Physics[J]: 2016, 16: 14687-14702.

McLinden, C., Olsen, S., Hannegan, B., et al. Stratospheric ozone in 3-D models: A simple chemistry and the cross-tropopause flux. Journal of Geophysical Research: Atmospheres[J]: 2000, 105: 14653-14665.

Nuryanto, D. E. Simulation of forest fires smoke using WRF-Chem model with FINN fire emissions in Sumatera. 1st International Symposium on Lapan-Ipb Satellite (Lisat) for Food Security and Environmental Monitoring[J]: 2015, 24: 65-69.

Oltmans, S. J., Lefohn, A. S., Harris, J. M., et al. Enhanced ozone over western North America from biomass burning in Eurasia during April 2008 as seen in surface and profile observations. Atmospheric Environment[J]: 2010, 44: 4497-4509.

Pacifico, F., Folberth, G., Sitch, S., et al. Biomass burning related ozone damage on vegetation over the Amazon forest: a model sensitivity study. [J]: 2015, 2015.

Paoletti, E.,Grulke, N. E. and Matyssek, R. Ozone Amplifies Water Loss from Mature Trees in the Short Term But Decreases It in the Long Term. Forests[J]: 2019, 11: 46.

Pope, R. J., Arnold, S. R., Chipperfield, M. P., et al. Substantial increases in Eastern Amazon and Cerrado biomass burning-sourced tropospheric ozone. Geophysical Research Letters[J]: 2020, 47: e2019GL084143.

Sadiq, M., Tai, A. P. K., Lombardozzi, D., et al. Effects of ozone-vegetation coupling on surface ozone air quality via biogeochemical and meteorological feedbacks. Atmospheric Chemistry and Physics[J]: 2017, 17: 3055-3066.

Schiferl, L. D. and Heald, C. L. Particulate matter air pollution may offset ozone damage to global crop production. Atmospheric Chemistry and Physics[J]: 2018, 18: 5953-5966.

Sitch, S., Cox, P. M., Collins, W. J., et al. Indirect radiative forcing of climate change through ozone effects on the land-carbon sink. Nature[J]: 2007, 448: 791-794.

Spitters, C. Separating the diffuse and direct component of global radiation and its implications for modeling canopy photosynthesis Part II. Calculation of canopy photosynthesis. Agricultural and Forest meteorology[J]: 1986, 38: 231-242.

Travis, K. R., Jacob, D. J., Fisher, J. A., et al. Why do models overestimate surface ozone in the southeastern United States? Atmospheric Chemistry and Physics[J]: 2016, 16: 13561.

Turetsky, M. R., Kane, E. S., Harden, J. W., et al. Recent acceleration of biomass burning and carbon losses in Alaskan forests and peatlands. Nature Geoscience[J]: 2011, 4: 27-31.

Val Martin, M., Logan, J. A., Kahn, R. A., et al. Smoke injection heights from fires in North America: analysis of 5 years of satellite observations. Atmospheric Chemistry and Physics[J]: 2010, 10: 1491-1510.

van der Werf, G. R., Randerson, J. T., Giglio, L., et al. Global fire emissions and the contribution of deforestation, savanna, forest, agricultural, and peat fires (1997-2009). Atmospheric Chemistry and Physics[J]: 2010, 10: 11707-11735.

Von Caemmerer, S. v. and Farquhar, G. D. Some relationships between the biochemistry of photosynthesis and the gas exchange of leaves. Planta[J]: 1981, 153: 376-387.

Vongruang, P.,Wongwises, P. and Pimonsree, S. Assessment of fire emission inventories for simulating particulate matter in Upper Southeast Asia using WRF-CMAQ. Atmospheric Pollution Research[J]: 2017, 8: 921-929.

Watson, G. L., Telesca, D., Reid, C. E., et al. Machine learning models accurately predict ozone exposure during wildfire events. Environmental Pollution[J]: 2019, 254: 112792.

Wiedinmyer, C., Akagi, S. K., Yokelson, R. J., et al. The Fire INventory from NCAR (FINN): a high resolution global model to estimate the emissions from open burning. Geoscientific

Model Development[J]: 2011, 4: 625-641.

Wittig, V. E., Ainsworth, E. A., Naidu, S. L., et al. Quantifying the impact of current and future tropospheric ozone on tree biomass, growth, physiology and biochemistry: a quantitative meta-analysis. Global Change Biology[J]: 2009, 15: 396-424.

Yan, Y.,Lin, J. and He, C. Ozone trends over the United States at different times of day. Atmospheric Chemistry and Physics[J]: 2018, 18: 1185.

Yue, X., Keenan, T. F., Munger, W., et al. Limited effect of ozone reductions on the 20-year photosynthesis trend at Harvard forest. Global Change Biology[J]: 2016, 22: 3750-3759.

Yue, X., Mickley, L., Logan, J., et al. Impact of 2050 climate change on North American wildfire: consequences for ozone air quality. Atmospheric Chemistry and Physics[J]: 2015, 15: 10033-10055.

Yue, X. and Unger, N. Ozone vegetation damage effects on gross primary productivity in the United States. Atmospheric Chemistry and Physics[J]: 2014, 14: 9137-9153.

Yue, X. and Unger, N. The Yale Interactive terrestrial Biosphere model version 1.0: description, evaluation and implementation into NASA GISS ModelE2. Geoscientific Model Development[J]: 2015, 8: 2399-2417.

Yue, X. and Unger, N. Fire air pollution reduces global terrestrial productivity. Nat Commun[J]: 2018, 9: 5413.

Zhang, L., Jacob, D. J., Downey, N. V., et al. Improved estimate of the policy-relevant background ozone in the United States using the GEOS-Chem global model with 1/2×2/3 horizontal resolution over North America. Atmospheric Environment[J]: 2011, 45: 6769-6776.

Zhou, S. S., Tai, A. P. K., Sun, S. H., et al. Coupling between surface ozone and leaf area index in a chemical transport model: strength of feedback and implications for ozone air quality and vegetation health. Atmospheric Chemistry and Physics[J]: 2018, 18: 14133-14148.

Zhu, J.,Tai, A. P. K. and Yim, S. H. L. Effects of ozone-vegetation interactions on meteorology and air quality in China using a two-way coupled land-atmosphere model. Atmos. Chem. Phys. Discuss. [preprint][J]: 2021, doi: https://doi.org/10.5194/acp-2021-165, 2021.

Ziemke, J. R., Chandra, S., Duncan, B. N., et al. Recent biomass burning in the tropics and related changes in tropospheric ozone. Geophysical Research Letters[J]: 2009, 36: L15819.

Table 1 Summary of simulations using the GC-YIBs model

Name	Emissions	O_3 damaging	O_3 sensitivities
CTRL_FIRE_HS	All including fires	Offline	High
CTRL_FIRE_LS	All including fires	Offline	Low
CTRL_NOFIRE_HS	All but without fires	Offline	High
CTRL_NOFIRE_LS	All but without fires	Offline	Low
O3CPL_FIRE_HS	All including fires	Online	High
O3CPL_FIRE_LS	All including fires	Online	Low
O3CPL_NOFIRE_HS	All but without fires	Online	High
O3CPL_NOFIRE_LS	All but without fires	Online	Low

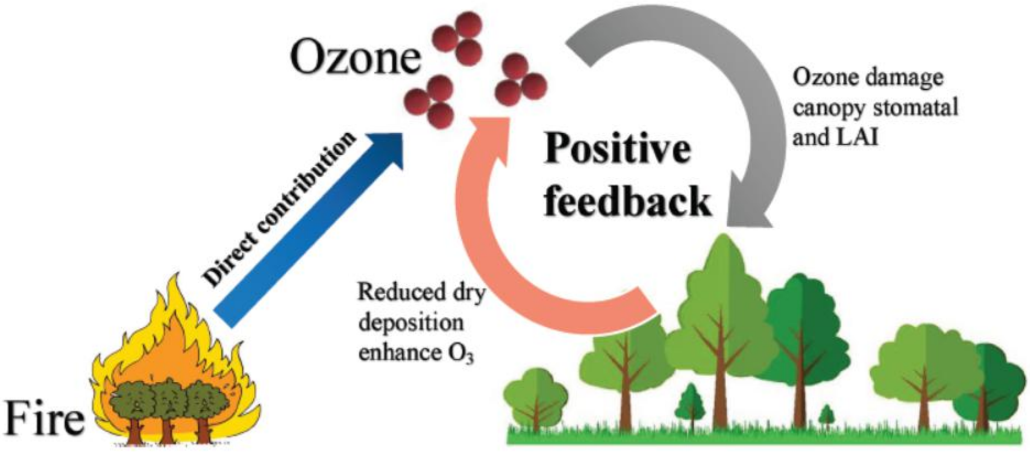

Figure 1 Diagram of the impacts of fires on surface O_3 through direct emissions and O_3-vegetation feedback.

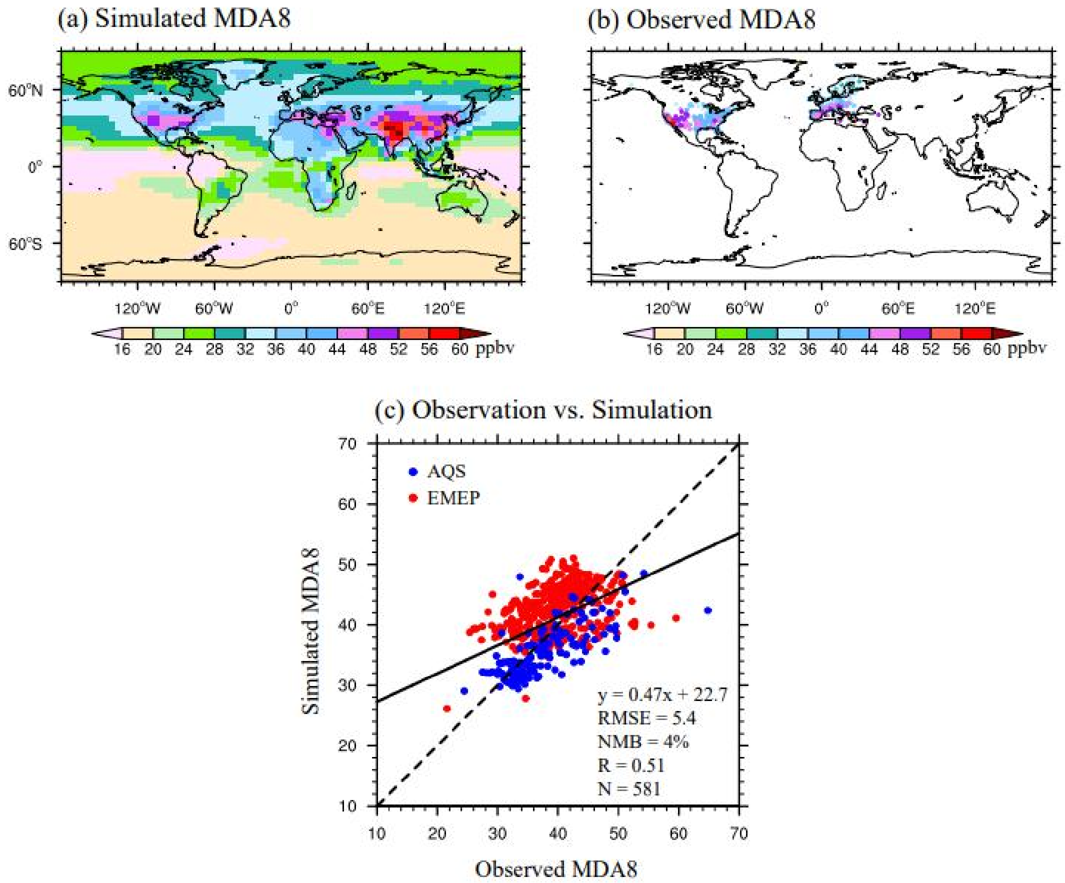

Figure 2 Spatial pattern of (a) simulated and (b) observed surface [O_3]. (c) Scatter plot of surface [O_3] over measurements in two regions. The black line shows the linear regression between the observed and simulated [O_3]. The regression fit, correlation coefficient (R), root mean square error (RMSE), and normalized mean bias (NMB) are shown in the bottom panel with an indication of site numbers (N) used for statistics.

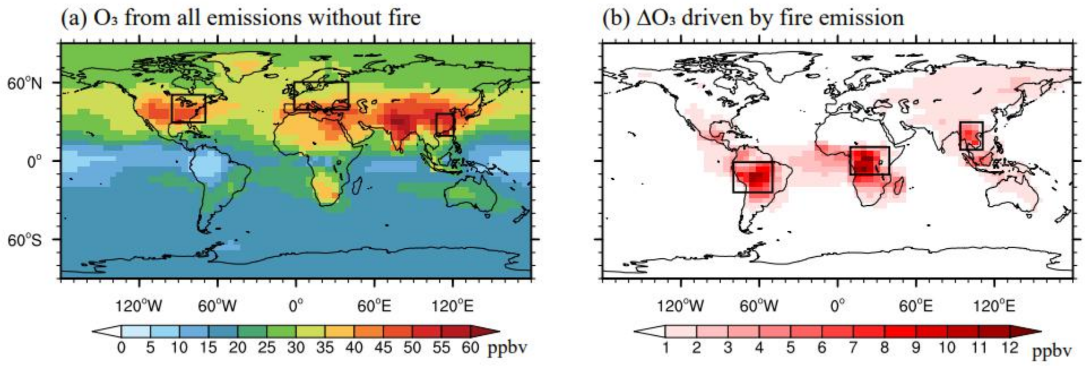

Figure 3 Annual surface [O_3] from (a) nonfire and (b) fire-alone sources. The six subregions are marked with black boxes: Eastern U.S. (EUS, 30°N-50°N, 95°W-70°W), Western Europe (WEU, 40°N-60°N, 0°-40°E), Eastern China (ECH, 20°N-35°N, 108°E-120°E), Amazon (AMZ, 25°S-0°, 80°W-50°W), Central Africa (CAF, 10°S-10°N, 10°E-40°E), and Southern Asia (SAS, 10°N-30°N, 95°E-110°E).

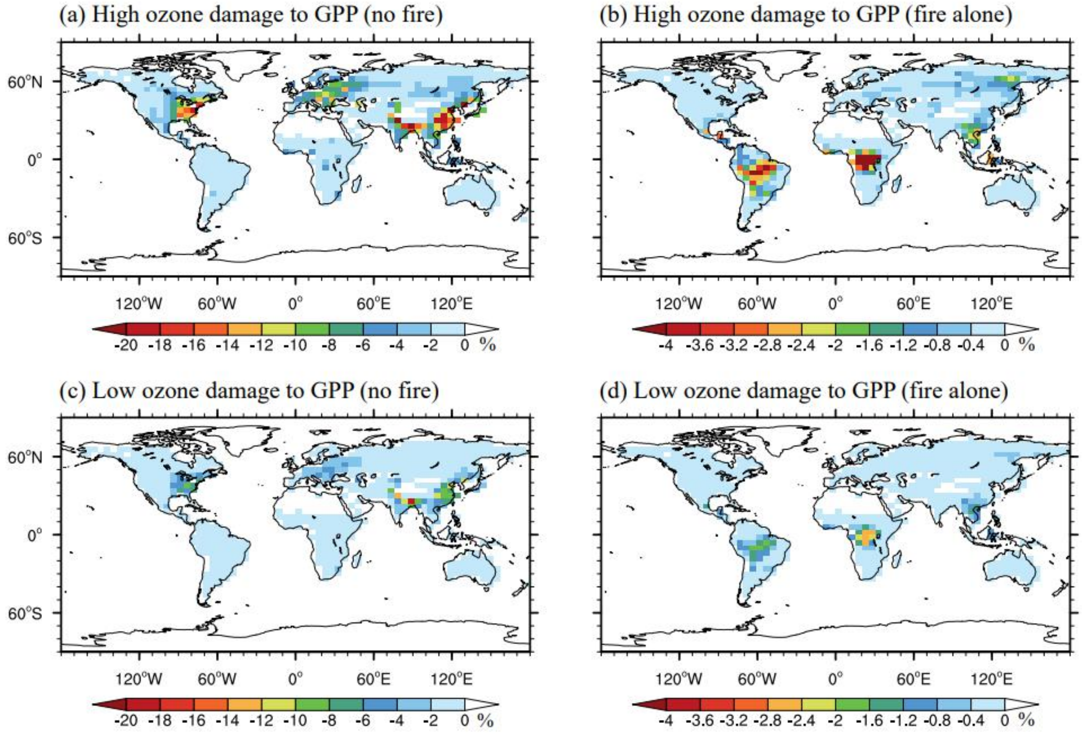

Figure 4 Annual percentage of reductions in GPP caused by O_3 from (a, c) nonfire and (b, d) fire alone sources with (a, b) high and (c, d) low O_3 sensitivities. Please note the differences in color scales.

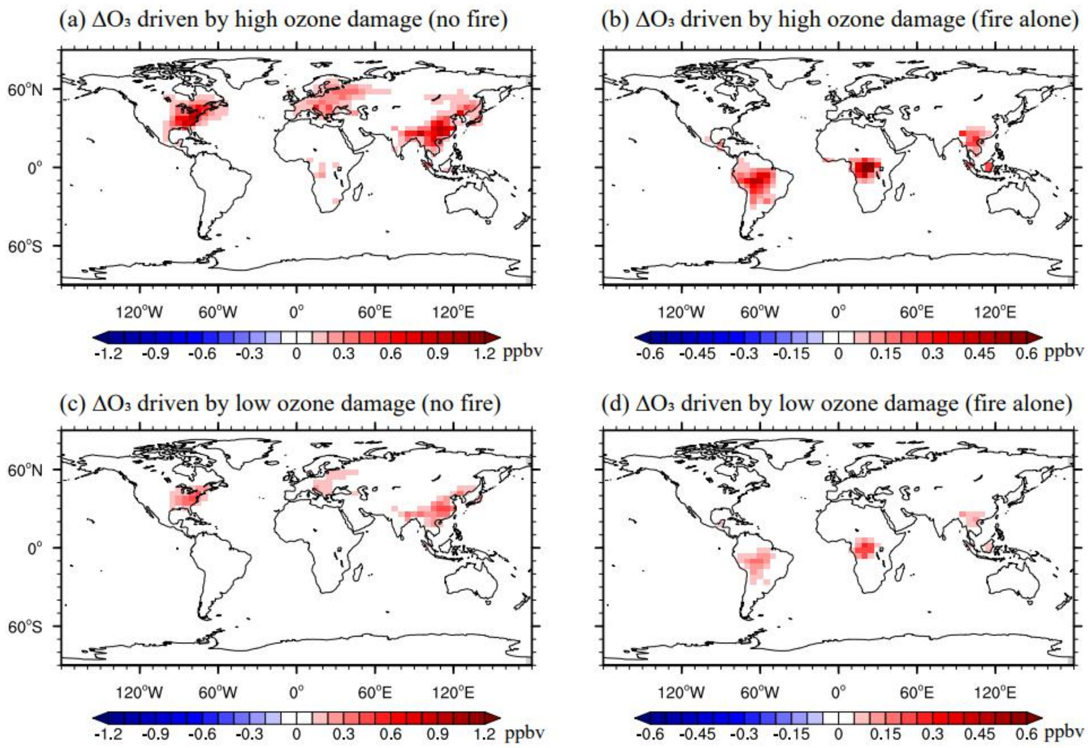

Figure 5 Annual feedback to surface O_3 caused by O_3 vegetation damage with (a, b) high and (c, d) low O_3 sensitivities. (a) and (c) represent feedback by O_3 from nonfire sources; (b) and (d) represent feedback by O_3 from fire emissions alone. Please note the differences in color scales.

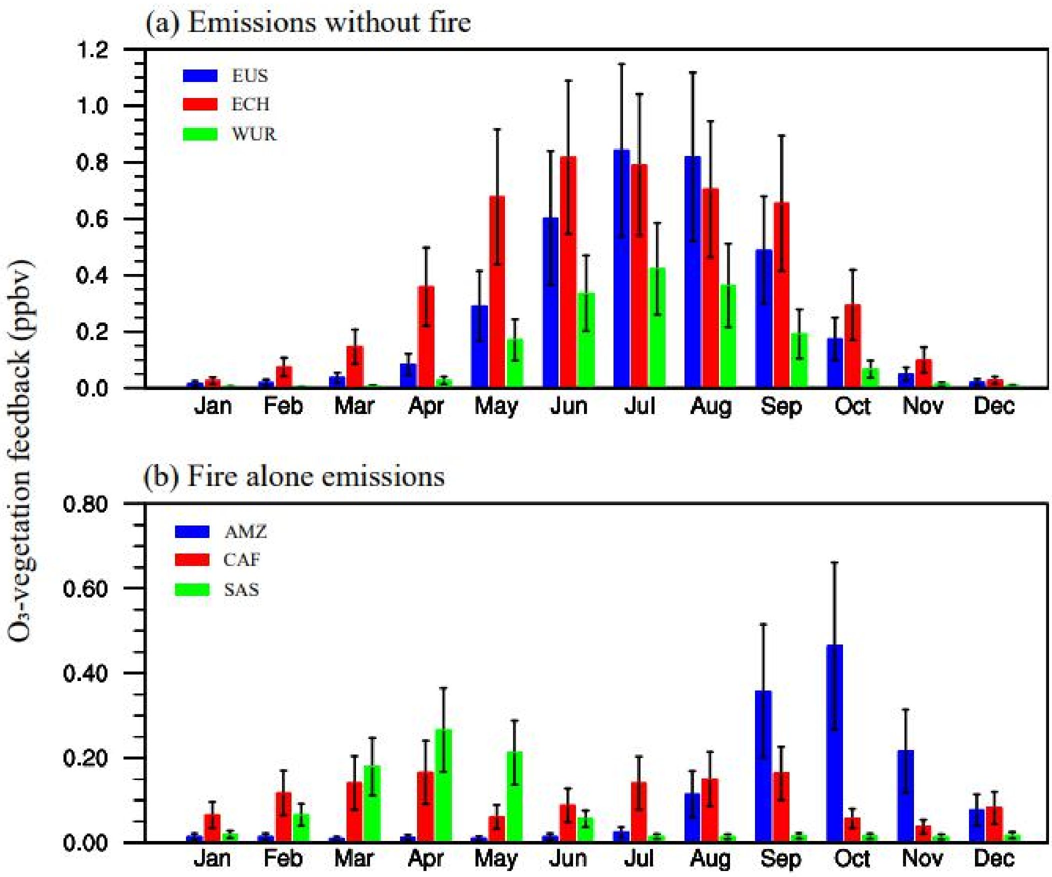

Figure 6 Seasonal variations in O_3-vegetation feedback driven by (a) nonfire and (b) fire-alone sources. The blue, red, and green bars in (a) represent the O_3-vegetation feedback in Eastern U.S. (EUS), Eastern China (ECH), Western Europe (WUR), respectively. The blue, red, and green bars in (b) represent the O_3-vegetation feedback in Amazon (AMZ), Central Africa (CAF), and Southern Asia (SAS), respectively. The error bars represent low to high O_3 damaging sensitivities.

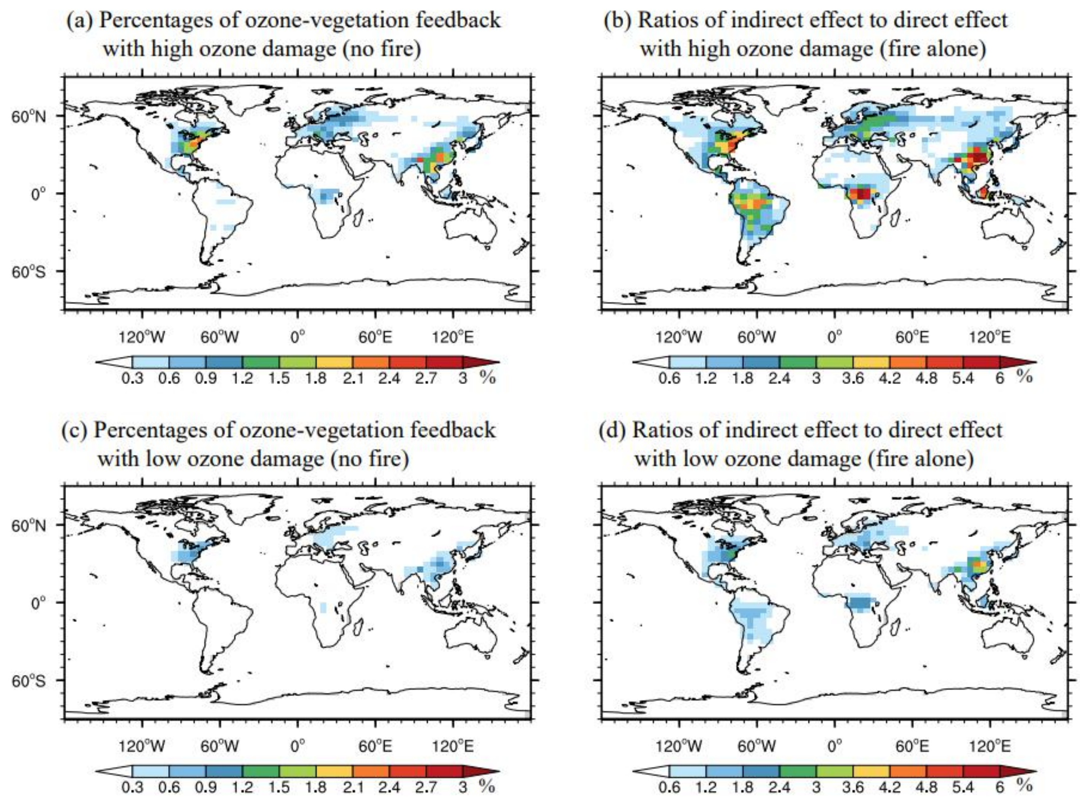

Figure 7 Annal ratios of indirect $\Delta[O_3]$ to ambient $[O_3]$ from (a, c) nonfire emissions and the ratios of indirect to direct $\Delta[O_3]$ from (b, d) fire emissions alone with (a, b) high and (c, d) low O_3 damaging sensitivities. Please note the differences in color scales.